Molecular Cell
Article

Lipid-Induced Conformational Switch Controls Fusion Activity of Longin Domain SNARE Ykt6

Wenyu Wen,[1,3] Jiang Yu,[3] Lifeng Pan,[3] Zhiyi Wei,[3] Jingwei Weng,[1,2] Wenning Wang,[1,2] Yan Shan Ong,[4] Ton Hoai Thi Tran,[4] Wanjin Hong,[4] and Mingjie Zhang[1,3,*]
[1]Institutes of Biomedical Sciences
[2]Department of Chemistry
Fudan University, Shanghai, P.R. China
[3]Department of Biochemistry, Molecular Neuroscience Center, Hong Kong University of Science and Technology, Clear Water Bay, Kowloon, Hong Kong, P.R. China
[4]Cancer and Developmental Cell Biology Division, Institute of Molecular and Cell Biology, Singapore 138673, Singapore
*Correspondence: mzhang@ust.hk
DOI 10.1016/j.molcel.2010.01.024

SUMMARY

While most SNAREs are permanently anchored to membranes by their transmembrane domains, the dually lipidated SNARE Ykt6 is found both on intracellular membranes and in the cytosol. The cytosolic Ykt6 is inactive due to the autoinhibition of the SNARE core by its longin domain, although the molecular basis of this inhibition is unknown. Here, we demonstrate that unlipidated Ykt6 adopts multiple conformations, with a small population in the closed state. The structure of Ykt6 in complex with a fatty acid suggests that, upon farnesylation, the Ykt6 SNARE core forms four α helices that wrap around the longin domain, forming a dominantly closed conformation. The fatty acid, buried in a hydrophobic groove formed between the longin domain and its SNARE core, is essential for maintaining the autoinhibited conformation of Ykt6. Our study reveals that the posttranslationally attached farnesyl group can actively regulate Ykt6 fusion activity in addition to its anticipated membrane-anchoring role.

INTRODUCTION

In eukaryotic cells, the dynamic trafficking of proteins and lipids between organelles is closely linked to membrane-bound vesicles that pinch off from one membrane and fuse with another (Jahn and Scheller, 2006; Südhof and Rothman, 2009). The specific targeting and fusion of different classes of transport vesicles to their distinct membrane destinations, which is essential to ensure the integrity and functions of organelles, relies on the precise pairing of cognate soluble *N*-ethylmaleimide-sensitive factor attachment protein receptors (SNAREs) anchored separately to the two membranes involved (Nicholson et al., 1998; Söllner et al., 1993; Weber et al., 1998). SNARE activity is governed in part by the conformational state of SNARE proteins. Most SNARE proteins contain three domains: a variable N-terminal regulatory domain, a conserved central 60–70 amino acid "SNARE core" that mediates the self-assembly of the four-helix-bundle SNARE core complex, and a C-terminal transmembrane domain (Sutton et al., 1998). In syntaxin SNAREs syntaxin-1 and Sso1p, the N-terminal three-helix-bundle Habc domain folds back and packs extensively with the SNARE core helix, preventing the SNARE core from freely forming the fusion-competent SNARE core complex (Dulubova et al., 1999; Misura et al., 2000; Munson et al., 2000; Nicholson et al., 1998). The N-terminal regulatory domain-mediated sequestration of the SNARE core is also observed in the nonsyntaxin SNARE Ykt6 (Hasegawa et al., 2004; Rossi et al., 2004; Tochio et al., 2001), although the molecular details of this autoinhibition are unclear.

Ykt6 is the most conserved and versatile SNARE (Rossi et al., 2004). Yeast Ykt6 is an essential protein involved in multiple membrane fusion reactions at the Golgi, vacuoles, and endosomes (Dilcher et al., 2001; Kweon et al., 2003; Lupashin et al., 1997; McNew et al., 1997; Meiringer et al., 2008; Ungermann et al., 1999). Mammalian Ykt6 is highly enriched in animal brains, and it forms specialized punctuates of unknown compartments in neurons (Hasegawa et al., 2003, 2004). In other mammalian cells, Ykt6 is found at the Golgi, perinuclear space, and cytosols (Fukasawa et al., 2004; Zhang and Hong, 2001). Unlike most other SNARE proteins, Ykt6 does not contain a transmembrane domain for stable membrane association. Instead, it contains a C-terminal "CCAIM" motif that can be palmitoylated at the first cysteine and farnesylated at the second cysteine (Figure S1A) (Fukasawa et al., 2004; McNew et al., 1997). A striking feature of Ykt6 is that it exists in both membrane-bound and soluble cytosolic pools, and functional Ykt6 requires the cycling of the protein between membranes and cytosol (Fukasawa et al., 2004; Hasegawa et al., 2003; McNew et al., 1997; Meiringer et al., 2008; Zhang and Hong, 2001). The stable membrane association requires both lipidations, and only membrane-anchored Ykt6 is fusion active (Fukasawa et al., 2004; Meiringer et al., 2008). The farnesylation of Ykt6 occurs posttranslationally and is essentially irreversible (Resh, 2006). Palmitoylation, instead, is a reversible and dynamic process (Dietrich and Ungermann, 2004; Linder and Deschenes, 2007; Meiringer et al., 2008). Thus, one might envision that single-lipidated (i.e., farnesylation at Cys195) Ykt6 exists in the cytosol and that cytosolic Ykt6 adopts an autoinhibited conformation via farnesyl-dependent interaction between its SNARE core and longin domain. The

cytosolic Ykt6 actively masks the long hydrophobic acyl chain of the farnesyl group via an intramolecular sequestration, as the acyl chain would otherwise be expected to insert into membrane bilayers. The palmitoylation of Cys194 increases the partition coefficient of Ykt6 to the hydrophobic membrane bilayers, thus shifting the protein from the cytosol to membranes (Fukasawa et al., 2004; Hasegawa et al., 2004; Meiringer et al., 2008). This palmitoylation-dependent cytosol-to-membrane shift is expected to be accompanied by the unmasking of the farnesyl group for membrane insertion as well as the conformational opening of the SNARE core for membrane fusion reactions. This model predicts that the farnesyl group in Ykt6 plays a dual role, namely both as a classical membrane localization signal and a direct SNARE activity regulatory switch. However, the above Ykt6 functional cycle model is not experimentally verified.

Here, we characterized the biochemical and structural properties of the full-length rat Ykt6 (rYkt6). We found that unlipidated Ykt6 adopts multiple interconverting conformational states in solution, spanning from the fully open form to the completely closed form. Guided by NMR spectroscopy, we discovered that the addition of a stoichiometric amount of a long acyl chain fatty acid-derived lipid shifted the protein into one homogenous conformation. High-quality Ykt6 crystals were readily obtained using the sample conditions derived from the NMR spectroscopic studies, and the structure of Ykt6 in complex with the lipid was solved to a high resolution. The results obtained in this work not only provide direct support for the Ykt6 functional cycling model, but also reveal exciting features of the coordinated actions of protein, lipid modifications, and membrane bilayers in controlling cellular functions of Ykt6.

RESULTS

Intramolecular Interaction between the Longin Domain and the SNARE Core of rYkt6

To examine whether rYkt6 adopts a closed conformation similar to its yeast counterpart, we compared the ^{1}H,^{15}N-HSQC spectra of rYkt6N (longin domain, residues 1–137) and rYkt6ΔC (Ykt6 without the ''CCAIM'' motif, residues 1–193) (Figure S1B). The full-length rYkt6 heavily aggregated even at a concentration below 10 μM, thus the protein is not amenable for detailed structural and biochemical analysis. The longin domain of rYkt6 adopts a well-defined conformation, as evidenced by the uniform and well-dispersed HSQC spectrum of the protein. Consistent with the direct interaction between the longin domain and the SNARE core of rYkt6, the inclusion of the entire SNARE core resulted in chemical shift changes to a large number of residues in the longin domain (Figure S1B). Thus, we suspect that rYkt6, like its yeast counterpart, adopts a closed conformation, with its SNARE core being sequestered by the longin domain. However, the poor NMR spectrum of rYkt6ΔC prevented us from further investigating the conformation of the protein.

DPC Binds to the Longin Domain of Ykt6

The longin domain of yeast Ykt6 was shown to directly bind to palmitoyl-CoA (Pal-CoA), thus mediating the palmitoylation of Vac8 (Dietrich et al., 2004). NMR spectroscopy was used to test for potential direct interactions between rYkt6N and Pal-CoA. Both Pal-CoA and palmitic acid micelles caused denaturation and precipitation of rYkt6ΔC (data not shown). To avoid protein denaturation, we lowered the concentrations of Pal-CoA and palmitic acid below their respective critical micelle concentrations (~40 μM for Pal-CoA and ~300 μM for palmitic acid) (Das and Hajra, 1992; Rys-Sikora and Gill, 1998). Under such conditions, no obvious direct interactions between rYkt6N and Pal-CoA/palmitic acid could be observed in our NMR-based assay. We screened several additional lipids for potential binding to rYkt6N and found that DPC (dodecylphosphocholine, with a critical micelle concentration of ~1.4 mM) weakly binds to rYkt6N (Figure 1A). The DPC binding site was mapped to the residues from αA and βE of rYkt6N (and yeast Ykt6N [data not shown]) through the chemical shift perturbation approach (Figure 1B). The DPC binding site of Ykt6N is hydrophobic in nature and overlaps with the previously identified SNARE core binding surface of the longin domain (Tochio et al., 2001).

DPC Stabilizes the Closed Conformation of rYkt6

Much to our surprise, the addition of stoichiometric amounts of DPC induced large chemical shift changes to many backbone amides in rYkt6ΔC; the protein is completely saturated in the presence of two molar ratios of DPC (Figure 1C, with dissociation constant (K_D) ~60 μM from the DPC titration), revealing that the full-length Ykt6 binds to DPC with a much higher affinity than does the longin domain alone. Mapping of the DPC binding-induced chemical shift changes of rYkt6ΔC onto the structure of its longin domain showed that DPC binds to the same hydrophobic site on the longin domain identified in rYkt6N, albeit DPC binding to rYkt6ΔC induced much more extensive chemical shift changes to the longin domain due to their stronger interaction (Figure 1B). The above data indicate that the SNARE core and the longin domain function synergistically in binding to DPC. The full-length yeast Ykt6 was also found to bind to DPC with a much higher affinity than its longin domain alone (data not shown).

The HSQC spectrum of rYkt6ΔC in the absence of DPC (Figure 2A, magenta peaks) revealed that each backbone amide for a number of residues displays several peaks, indicating that the protein exists in multiple conformations exchanging at slow-to-intermediate timescales. The exquisite sensitivity and resolution of NMR chemical shifts allow us to observe that one of these conformations coincides with the fully open structure, as the amide peaks of this state overlap well with the corresponding amides of the longin domain of the protein (Figure 2A, green peaks). Another conformation of rYkt6ΔC matches with the structure of the protein saturated with DPC (Figure 2A, black peaks), and this conformer represents the completely closed state of the protein (see below for details). The rest of the conformations of rYkt6ΔC are between the fully open and completely closed state of the protein. We conclude that the unlipidated full-length Ykt6 is highly dynamic, with conformations ranging from the fully open to the completely closed states interconverting in solution.

The addition of up to two molar ratios of DPC (~0.4 mM) to rYkt6ΔC completely saturated the protein (Figures 1C and 2A). The NMR spectrum of DPC-saturated rYkt6ΔC is highly homogeneous and fits with a single conformation (Figure 1C). The

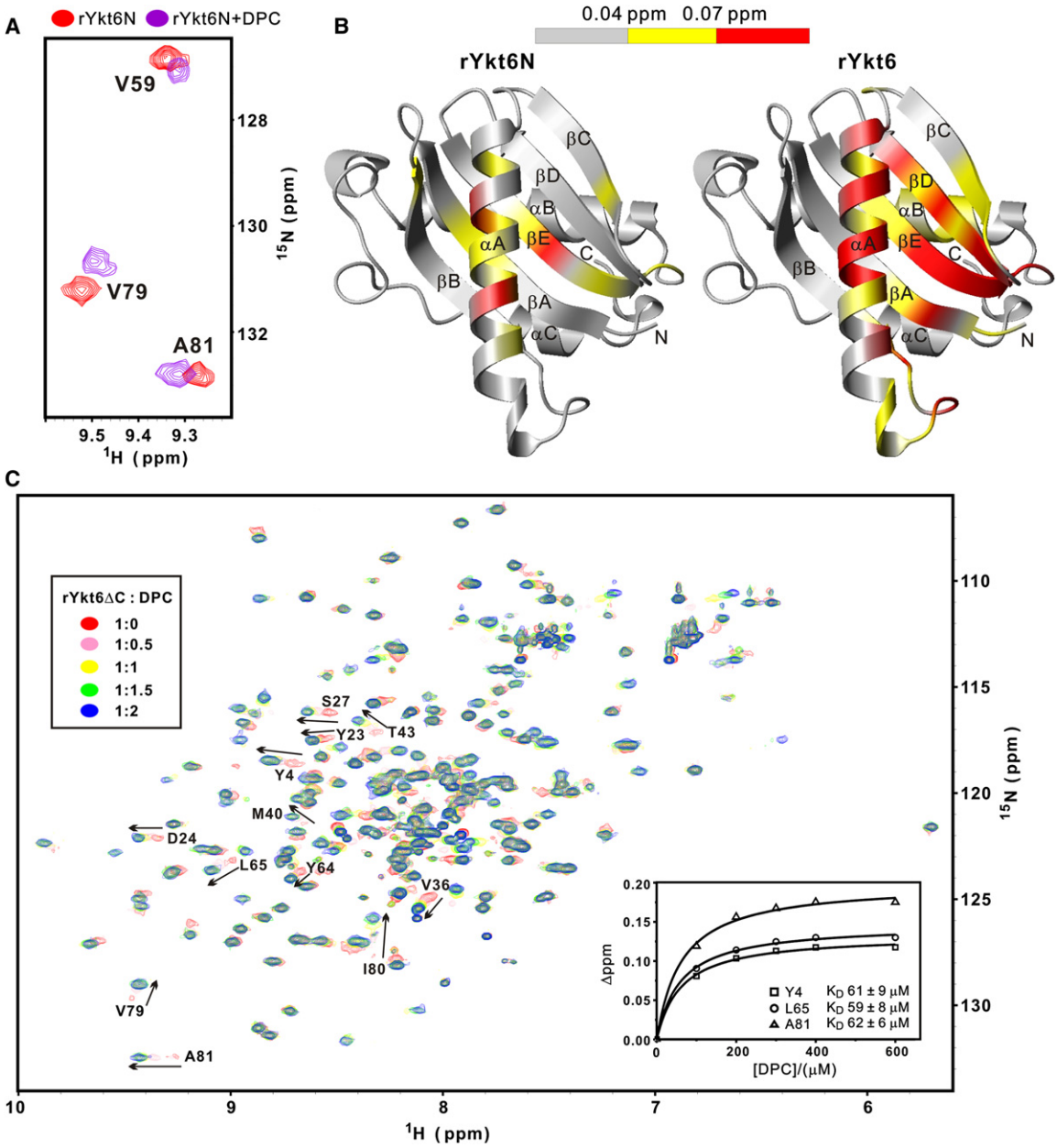

Figure 1. DPC Binds to rYkt6

(A) Selected region of the ^{1}H,^{15}N-HSQC spectra of the rYkt6 longin domain (~0.2 mM) in the absence (red) and presence (purple) of four molar ratios of DPC.

(B) Summary of the chemical shift changes of rYkt6N (left panel) and rYkt6ΔC (right panel) induced by DPC binding (see also Figure S1). The combined ^{1}H and ^{15}N chemical shift changes are defined as: $\Delta_{ppm} = [(\Delta\delta_{HN})^2 + (\Delta\delta_N \times \alpha_N)^2]^{1/2}$. $\Delta\delta_{HN}$ and $\Delta\delta_N$ represent chemical shift differences of amide proton and nitrogen chemical shifts of rYkt6N upon DPC binding. The scaling factor (α_N) used to normalize the ^{1}H and ^{15}N chemical shifts is 0.17. The coloring scheme is represented using a horizontal bar at the top.

(C) NMR-based titration of rYkt6ΔC (~0.2 mM) with increasing concentrations of DPC. The insert shows the dose-dependent titration curves of several representative backbone amides of rYkt6ΔC as a function of DPC concentration. The dissociation constants of the rYkt6ΔC/DPC derived from the binding curves are shown in the insert. The chemical shift assignments of selected peaks of rYkt6ΔC were transferred from those of rYkt6N.

most straightforward explanation for the above findings is that DPC binds and subsequently stabilizes the closed conformation. Analytical ultracentrifugation-based studies of rYkt6ΔC with and without DPC confirmed our interpretation. In the absence of DPC, rYkt6ΔC displays a broad peak with a monomeric molecular mass of ~22 kDa in the continuous sedimentation coefficient distribution analysis, consistent with the existence of multiple, interconverting conformational states of the protein. In the presence of DPC, rYkt6ΔC shows as a much sharper monomer peak in the same sedimentation velocity analysis, indicating

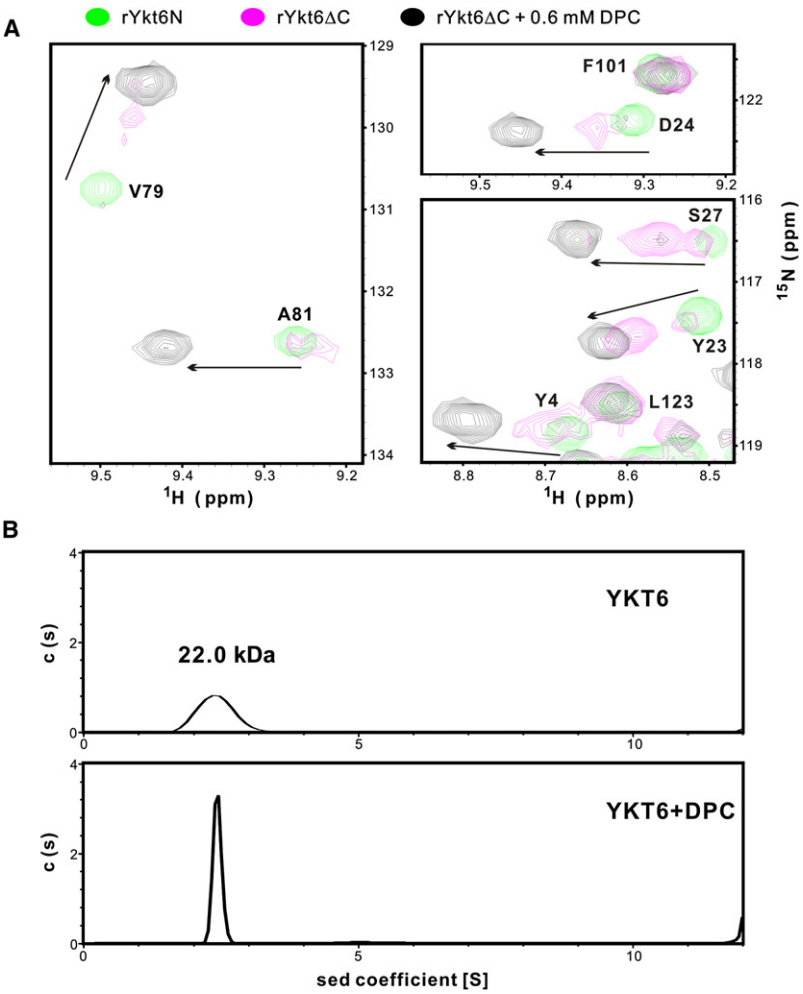

Figure 2. DPC Binding Stabilizes the Closed Conformation of the Full-Length rYkt6

(A) Superposition plot of ^{1}H,^{15}N-HSQC spectra of the rYkt6 longin domain (0.2 mM, green) and rYkt6ΔC (0.2 mM) in the absence (magenta) and presence of 0.6 mM DPC (black). For clarity, only a selected region of the spectra is shown.

(B) Sedimentation velocity analysis of rYkt6ΔC (40 μM) in the absence (left panel) and presence of 0.6 mM DPC (right panel). The calculated molecular mass of the protein is indicated.

that the rYkt6ΔC/DPC complex adopts a more compact structure in solution than rYkt6 alone (Figure 2B). Importantly, it has been shown that the farnesylated Ykt6 also adopts a more compact monomeric structure than its unlipidated counterpart (Pylypenko et al., 2008).

Crystal Structure of rYkt6 in the Closed Conformation

The excellent NMR spectrum of rYkt6ΔC in the presence of stoichiometric ratios of DPC indicates that, under these conditions, the protein exists in a stable and monodispersed conformational state, which should be favorable for forming protein crystals. Guided by this information, we succeeded in obtaining high-quality rYkt6ΔC crystals by simply mixing the protein sample in the presence of ~1 mM DPC with ammonium sulfate. The structure of rYkt6ΔC in complex with DPC was solved at 2.4 Å resolution (Table 1).

The electron densities of the entire length of rYkt6ΔC are clearly defined. As in its isolated state, the longin domain in the full-length rYkt6 possesses a five-stranded (βA–βE) antiparallel β sheet, sandwiched by αA on one side and αB/αC on the other (Figures 3A and 3B, green ribbon). The overall conformation of the longin domain in rYkt6ΔC is highly similar to that of the isolated longin domain (Figure 3B). The entire Ykt6 SNARE core is well defined and wraps around the longin domain, causing the full-length rYkt6 to adopt a fully closed conformation with a compact globular shape (Figure 3). The rYkt6 SNARE core adopts a conformation distinct from all previously characterized SNARE cores, either in their N-terminal regulatory domain-sequestered forms or in the fusion-competent four-helix bundles (Dulubova et al., 1999; Misura et al., 2000; Munson et al., 2000; Nicholson et al., 1998; Sutton et al., 1998). Instead of adopting a single extended α helix, the rYkt6 SNARE core consists of four well-separated α helices (αD–αG) and a short β strand (βF) connecting αD and αE (Figures 3A and 3B, pink ribbon). Although the SNARE core of syntaxin 1a in complex with nSec1 forms three closely spaced α helices (Misura et al., 2000), such SNARE core helix breakage can be viewed as a local deformation of the long SNARE core helix induced by nSec1 binding and is radically different from the interspaced multihelix conformation of the Ykt6 SNARE core. The C-terminal halves of the SNARE cores from syntaxin 1 and Sso1p have been found to be rather flexible in solution (Dulubova et al., 1999; Fiebig et al., 1999), whereas the entire SNARE core of rYkt6 is well folded. Additionally, the SNARE core of Ykt6 immediately follows its longin domain; therefore, Ykt6 lacks the linking helices observed between the N-terminal Habc domain and the SNARE core in syntaxin family SNAREs (Dulubova et al., 1999; Misura et al., 2000; Munson et al., 2000; Nicholson et al., 1998; Sutton et al., 1998). Finally, the structure of the Ykt6 SNARE core is distinct from the recently reported crystal structure of another longin SNARE Sec22b, in which only a small portion of the SNARE motif (the βF–αD region; see below for details) is defined (Mancias and Goldberg, 2007); this difference may be correlated with the activity differences of these two SNAREs (i.e., Ykt6 is rather tightly regulated by its autoinhibition mechanism and Sec22b adopts a largely open conformation) (Gonzalez et al., 2001; Liu et al., 2004; Tochio et al., 2001).

The Longin Domain/SNARE Core Interface

The entire SNARE core of Ykt6 is involved in its longin domain/SNARE core interface, covering nearly half of the longin domain

Table 1. X-Ray Data Collection and Refinement Statistics

Data collection	
Space group	$C222_1$
Unit cell (Å)	a = 54.81, b = 59.71, c = 108.33, α = β = γ = 90°
Resolution (Å)	30.0–2.44 (2.51–2.44)
Observed reflections	35,476
Unique reflections	6900
R_{merge} [a] (%)	6.7 (33.6)
I/σ	10.0 (2.2)
Average redundancy	5.1 (5.2)
Completeness (%)	100.0 (100.0)
Refinement	
R_{work} [b]/ R_{free} [c] (%)	19.9/26.1
No. atoms	1659
Proteins	1540
Ligand/ion	33
Water	86
Mean B factors (Å^2)	33.7
Proteins	32.8
Ligand/ion	66.1
Water	36.3
Rmsds	
Bond length (Å)	0.007
Bond angles (°)	1.060
Ramachandran plot (%)	
Most favored	94.9
Additionally allowed	5.1

The values in parentheses refer to the highest-resolution shell.
[a] $R_{merge} = \Sigma|I_i - I_m|/\Sigma I_i$, where I_i is the intensity of the measured reflection and I_m is the mean intensity of all symmetry-related reflections.
[b] $R_{factor} = \Sigma h \mid |F_{obs}| - |F_{calc}| \mid / \Sigma |F_{obs}|$, where $|F_{obs}|$ and $|F_{calc}|$ are the observed and calculated structure factor amplitudes, respectively. Summation includes all reflections used in the refinement.
[c] $R_{free} = \Sigma \mid |F_{obs}| - |F_{calc}| \mid / \Sigma |F_{obs}|$, evaluated for a randomly chosen subset of 10% of the diffraction data not included in the refinement.

surface (Figure 3C). Residues 141–147 of the SNARE core form helix αD, which packs with the N-terminal end of αB in the longin domain; residues 152–154 form β strand F, which pairs in parallel with βC of the longin domain; residues 157–160 form a single-turn helix (αE) that contacts with αA and βC through hydrophobic interactions; finally, residues 167–190 form an α helix hairpin (αF and αG) that makes extensive contact with the entire αA helix (Figure 3).

The longin domain/SNARE core interface of Ykt6 can be divided into three distinct regions based on the SNARE core's organization (Figures 4A and 4B): (I) the C-terminal two helices (αF and αG) and the αE/αF loop, (II) the central βF region and the following αE helix, and (III) the C-terminal half of αD and the αD/βF loop of the SNARE core. In region I, the hydrophobic residues from the two amphipathic helices (αF and αG) make numerous contacts with the hydrophobic residues from the longin domain. It is safe to assume that the extensive interactions in this region play a vital role in keeping the SNARE core in a closed conformation. In addition to the hydrophobic interactions, Glu165 from the core forms a salt bridge with Arg50 from the longin domain. Asp168, Tyr185, and Arg189 from αF and αG interact with each other via hydrogen bonding and charge-charge interactions, thereby stabilizing the αF/αG hairpin (Figure 4B, top panel). The interaction in region II is mainly mediated by backbone hydrogen bonds formed between βF of the SNARE core and βC of the longin domain and hydrophobic contacts between residues from αE and αA. Ile151 from the αD/βF loop and Ile152 in βF also contribute to the binding by making contact with Phe91 and Ala57 from the longin domain, respectively (Figure 4B, central panel). The interactions in region III are rather loose. Leu146 from αD interacts with Phe91 from αB of the longin domain. The salt bridge and the hydrogen bonds formed between the side chains Arg56, Glu95, and Thr149 also contribute to the interactions in region III.

DPC Binding Pocket in the Full-Length Ykt6

Despite relatively weak X-ray diffraction signals often encountered for prenyl groups in prenylated proteins (Pylypenko et al., 2008), we were able to trace one DPC molecule with high confidence in each Ykt6 molecule (Figure 5A). The DPC molecule binds to a semiopen hydrophobic groove situated between the helices αF/αG of the SNARE core and the concave hydrophobic surface of the longin domain (Figures 5B and 5C). The amino acid residues forming this DPC-binding hydrophobic groove are highly conserved (Figure S2A). The NMR-based DPC titration experiments showed that DPC directly binds to this pocket (Figure 1). It is clear from the structure that the full-length Ykt6 binds to DPC with a much higher affinity than the longin domain alone, as the interaction between the login domain and the SNARE core together creates a semiopen hydrophobic pocket for DPC binding (Figure 5C).

In the Ykt6/DPC complex, the entire aliphatic tail of DPC (shown in green in Figures 5A and 5C) inserts into the hydrophobic pocket of Ykt6. The polar head group of DPC is in close proximity with the C terminus of αG and is solvent exposed. Therefore, the orientation of the protein-bound DPC fits well with the farnesyl group attached to Cys195 of Ykt6 (Figure 5A). Under cellular conditions, Ykt6 is constitutively farnesylated at Cys195 by the formation of a thioether linkage. The aliphatic tail of farnesyl is more bulky and rigid than that of DPC, as the farnesyl group contains three more carbon atoms and the aliphatic chain is unsaturated and branched. Additionally, the formation of the thioether linkage effectively extends the length of the hydrophobic chain of the farnesyl group by including the side chain of Cys195 (Figure S3). Therefore, it is likely that a farnesyl group binds to Ykt6 with an affinity higher than that of DPC. The intramolecular interaction between Cys195-linked farnesyl group and Ykt6 would further enhance the interaction between the lipid moiety and the protein. We built a structural model of Cys195-farnesylated Ykt6 structure by first manually superimposing the farnesyl tail with the tail of DPC shown in Figure 5A. The manually built Cys195-farnesylated Ykt6 structural model was then energy minimized first using the program Haddock (Dominguez et al., 2003). In this energy-minimized structure, the hydrophobic tail

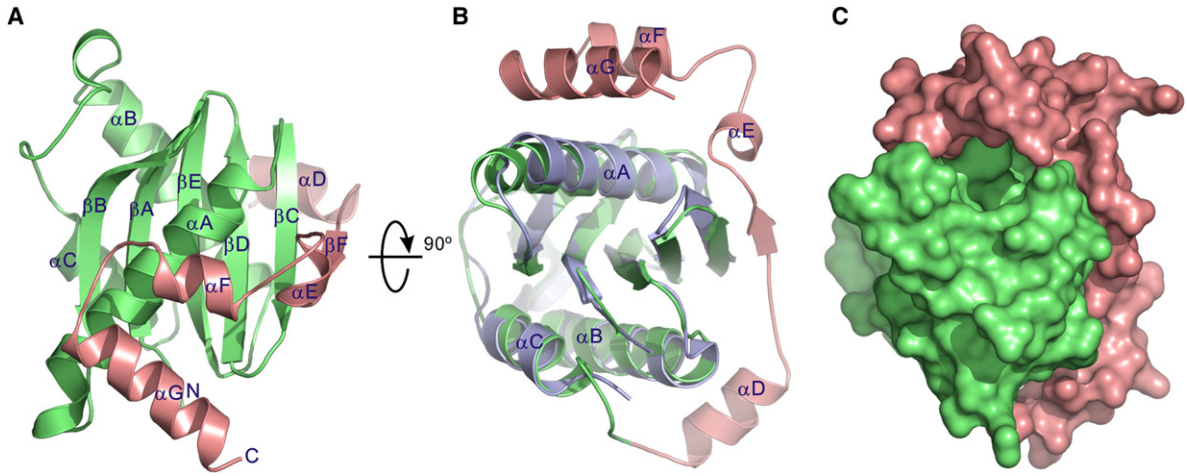

Figure 3. Crystal Structure of rYkt6ΔC

(A and B) Ribbon diagram of rYkt6ΔC with the longin domain colored in green and the SNARE core in pink, viewed from the top (A) and the side (B). For comparison, the structure of yeast Ykt6 longin domain (light blue, PDB ID number 3BW6) is superimposed to the longin domain of rYkt6ΔC, showing that the binding of the SNARE does not induce significant conformational changes to the longin domain.

(C) Surface representation of rYkt6ΔC with the same coloring scheme and orientation as in (B).

of the farnesyl group occupied the hydrophobic groove of Ykt6 (Figure S3A). This structure was then subjected to molecular dynamics simulations. The final simulated farnesylated Ykt6 structural model is shown in Figures S3B–S3D. In this model, the Cys195-attached farnesyl group further extends into the hydrophobic pocket of Ykt6, likely as a result of lengthening of the hydrophobic chain due to the formation of the thioether bond. The C-terminal αG and αF helices undergo some conformational changes, leading to a narrower farnesyl-binding hydrophobic groove (Figures S3B and S3C). The farnesyl group fits snugly into this hydrophobic groove, and the remaining space in the hydrophobic groove is not large enough to accommodate a palmitoyl group (Figures S3C and S3D). Considering that Ykt6 is farnesylated first, and the farnesyl group is constitutively attached to the protein, we believe that the Ykt6/DPC complex structure presented here best represents the structure of the farnesylated Ykt6. The Ykt6/DPC complex structure further indicates that the farnesylated, unpalmitoylated Ykt6 adopts a fully closed conformation soluble in the cytoplasm, as the farnesyl group is completely buried in the hydrophobic core of the protein.

Structural Comparison of rYkt6 with Other Longin SNAREs

In addition to Ykt6, two longin SNAREs, Sec22 and VAMP7, have also been shown to adopt a folded-back autoinhibited conformation (Mancias and Goldberg, 2007; Martinez-Arca et al., 2003; Pryor et al., 2008; Tochio et al., 2001). In the crystal structure of the Sec22/Sec23/Sec24 complex, a ten-residue SNARE core fragment (from −4 to −1 region of the SNARE core, corresponding to the βF–αE region in Ykt6) was found to adopt a stable conformation, with a three-residue β strand followed by a short α helix (Mancias and Goldberg, 2007) (summarized in Figure 4D). In the isolated Sec22, no interactions between the SNARE core and the longin domain could be observed (Gonzalez et al., 2001), and the SNARE core is likely to adopt a fully open conformation. Interestingly, the interaction between the N-terminal part of the ArfGAP Hrb and the longin domain of VAMP7 also resembles the interactions between the SNARE core fragment and the longin domain observed in Ykt6 and Sec22 (i.e., each form a short β strand followed by a single-turn α helix) (Figure 4D) (Pryor et al., 2008). It has been shown that the SNARE core of VAMP7 competes with Hrb for binding to the longin domain, presumably due to the binding of the SNARE core to the same site on the longin domain of VAMP7 (Martinez-Arca et al., 2003; Pryor et al., 2008). As indicated in the superimposition analysis in Figure 4D, the C-terminal ends of the αA helix and the βC strand of each longin domain provide a hydrophobic surface to interact with hydrophobic residues from the −4 to −1 region of their respective SNARE core region (and to the N-terminal end of Hrb in the case of VAMP7). The hydrophobic residues that are key for the formation of the interface between each longin domain and its corresponding SNARE core are all conserved in the three longin family SNAREs (Figure 4E). These residues also align well with those in Hrb bound by the VAMP7 longin domain. Thus, the autoinhibitory conformation is likely to be a general structural feature for longin SNAREs, with the conformational opening of each SNARE being regulated by the interaction between the longin domain and its SNARE core. However, the strengths of this autoinhibition among the longin SNAREs are likely to be very different. We believe that Ykt6 adopts a dominantly closed conformation in its farnesylated state due to the extensive interaction between the entire SNARE core, the farnesyl group, and its longin domain. In contrast, in Sec22b, VAMP7, and Nyv1p, the interaction between the longin domain and the SNARE core is limited to βF and αE of the SNARE core and one edge (βC side) of the longin domain. The lack of interactions between the C-terminal part of the SNARE core (from 0 to +8 region) and the longin domain in Sec22b and Nyv1p (Gonzalez et al., 2001; Wen et al., 2006) can be attributed to the lack of

key hydrophobic residues found in the αA helix of Ykt6 (Phe39, Phe42, and Leu46 in Ykt6, which form numerous contacts with αF and αG of the SNARE core) (Figure S2). VAMP7 also lacks these critical hydrophobic residues in its αA helix. Therefore, Sec22b, VAMP7, and Nyv1p are likely to adopt dominantly open conformations in their isolated states, and the open-closed conformational equilibrium may be influenced by the binding of different coat complexes to each SNARE due to the low energy barrier between their open and closed conformations (Liu et al., 2004; Mancias and Goldberg, 2007; Pryor et al., 2008; Wen et al., 2006). Since Ykt6 lacks a transmembrane domain C-terminal to its SNARE core, the protein is mainly localized in cytosol (Fukasawa et al., 2004; Meiringer et al., 2008). The cytosolic Ykt6 is potentially accessible to all types of membranes by simple diffusion and thus should be kept at a tightly autoinhibited state to prevent the occurrence of nonspecific SNARE pairing. In contrast, for longin SNAREs that are constitutively membrane-attached through their respective transmembrane domains (e.g., Sec22b, VAMP7, and Nyv1p), a more open conformation may be advantageous, so that cognate SNARE pairing can readily occur once they meet each other. Thus, the distinct conformational features of Ykt6 are likely the results of its unique cellular functional requirements.

Ykt6-Medaited SNARE Complex Assembly Depends on Intramolecular Interactions between Its Longin Domain, Its SNARE Core, and the Lipid Moiety

Next, we investigated the roles of selected amino acid residues in the hydrophobic groove responsible for the interactions between the longin domain, the SNARE core, and DPC (or the farnesyl group). To probe the longin/SNARE core interaction, we chose Phe42 at the middle of αA of the longin domain and V171 from αF of the SNARE core, as both residues are critical for the hydrophobic packing of the SNARE core and the longin domain, but are not in direct contact with Ykt6-bound DPC (Figures 4B and 5B). The substitution of either of the two residues with glutamic acid led to a smaller elution volume than the wild-type protein on an analytic gel filtration column, indicating that each mutant adopts a more open conformation than the wild-type protein (Figure S4A). Consistent with this observation, analytical ultracentrifugation analysis showed that both F42E and V171E mutants displayed much broader peaks compared to the wild-type protein (Figure 6, left panels). Upon addition of DPC, the peaks of these two mutants on the sedimentation coefficient distribution profiles became sharper, but were not as sharp as that of the wild-type protein, indicating that both mutants can still bind to DPC, albeit with weaker binding affinities than the wild-type protein (Figure 6, right panels). The above data further indicate that the longin domain, the SNARE core, and the bound DPC (or the farnesyl group) are mutually coupled in the formation of the closed conformation of Ykt6.

To evaluate the residues in the farnesyl group binding pocket, we substituted Tyr64 with glutamic acid, as it is on the surface of the lipid binding pocket. The Y64E mutant, like the F42E and V171E mutants, was eluted at a smaller volume on the analytic gel filtration column and had a broader peak in the analytical ultracentrifugation analysis, indicating that the mutation lead to a more open conformation of the protein, presumably due to the disruption of the hydrophobic interaction network in the region (Figures 6 and S4A). We next evaluated Tyr185 in the αG of the SNARE core, as this residue is expected to stabilize the packing between αF and αG of the SNARE core as well as participate the longin/SNARE core/lipid interactions (Figures 4A and 5B). Unlike the rest of the mutants described above, the Y185E mutant of Ykt6 was eluted at a slightly smaller volume on the analytic gel filtration column and displayed a sharper peak on the analytical ultracentrifugation analysis (Figures 6 and S4A), indicating that the mutant has a more compact conformation than the wild-type protein in the absence of DPC. The side chain of Tyr185 forms a hydrogen-bonding network together with Asp168 and Arg189, thereby stabilizing the packing between αF and αG of the SNARE core (Figures 4). The substitution of Tyr185 with glutamic acid is expected to strengthen the packing between αF and αG due to the formation of additional salt bridges between Arg189 and Glu185. On the other hand, the substitution of Tyr185 with glutamic acid would place a negatively charged group at the center of the lipid-binding hydrophobic groove of Ykt6. Therefore, the Y185E mutant should possess weaker lipid interactions. As predicted, analytical ultracentrifugation analysis showed that the Y185E mutant displayed somewhat weaker DPC binding than the wild-type protein (Figure 6). The substitution of Tyr185 with glutamic acid may have a larger impact on the protein's binding to the bulkier farnesyl group, as the farnesyl tail is expected to be closer to the negatively charged glutamic acid than the DPC tail (Figure S3). As a control, we demonstrated by circular dichroism spectroscopy that all the above mutations do not alter the overall folding of the proteins (Figure S4B).

To establish a correlation between the closed-open conformational equilibrium of Ykt6 and its cellular function, we first compared the cellular localization patterns of the wild-type Ykt6 with those of its various mutants described above. Consistent with published observations (Fukasawa et al., 2004; Hasegawa et al., 2003, 2004), the full-length rYkt6 showed a predominantly diffused pattern in both cytosols and nuclei when overexpressed in HeLa cells, consistent with a fully closed conformation of the protein with the farnesyl group sequestered from interacting with membranes (Figure 7A). Each of the Ykt6 mutants (F42E, V171E, Y64E, and Y185E) with compromised lipid binding capacities showed dramatically different localization patterns from the wild-type protein. These Ykt6 mutants are mainly localized at the perinuclear regions, which have been suggested to be the Golgi apparatus (Fukasawa et al., 2004), and punctuate organelle membranes (Figures 7B–7E). Biochemical fractionation experiment showed that, in contrast to the wild-type protein, these mutants are significantly membrane-bound (Figure 7F), presumably due to the mutation-induced shifting of each Ykt6 mutant to a more open conformation. We next performed a SNARE complex assembly assay to assess the conformational status of the wild-type Ykt6 and its mutants, shown in Figures 7A–7E. Mammalian Ykt6 has been shown to form SNARE complex with Bet1, syntaxin 5, and GS28 (Zhang and Hong, 2001). We compared the Ykt6-mediated SNARE complex assembly of the wild-type Ykt6 and its mutants by probing the amount of endogenous Bet1 bound to GFP-tagged Ykt6 transiently expressed in HeLa cells

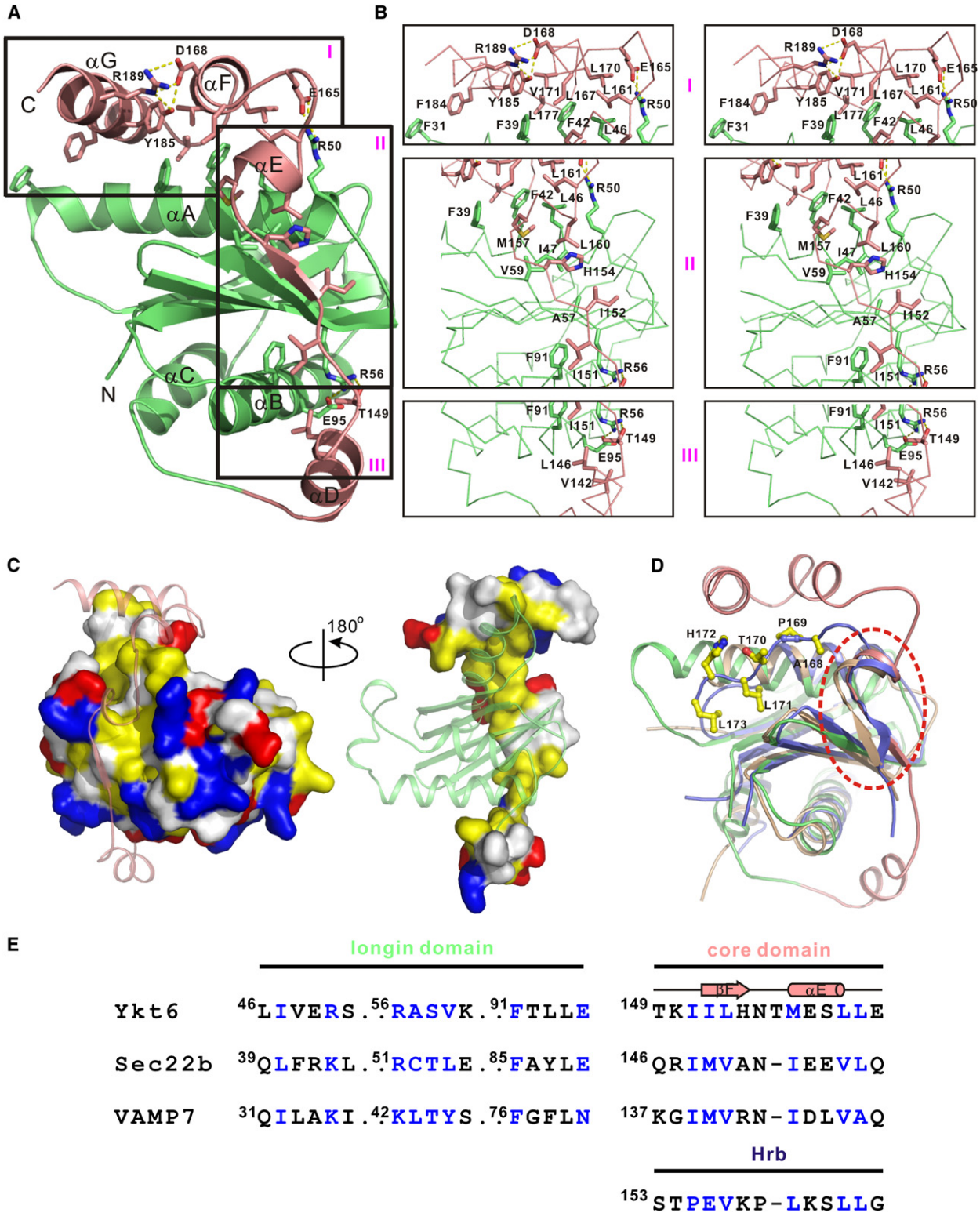

Figure 4. The Longin Domain/SNARE Core Interface of Ykt6

(A) The longin domain/SNARE core interface is divided into three regions (I, II, and III) according to the interaction features of the SNARE core.

(B) Stereo views showing the interaction details of the three regions of the longin domain/SNARE core interface indicated in (A). In this drawing, the backbone of rYkt6ΔC is drawn in line model, with the longin domain colored in green and the SNARE core in pink. The side chains of the residues involved in the interdomain interactions are drawn in stick model. Charge-charge and hydrogen bonding interactions are highlighted by yellow dashed lines.

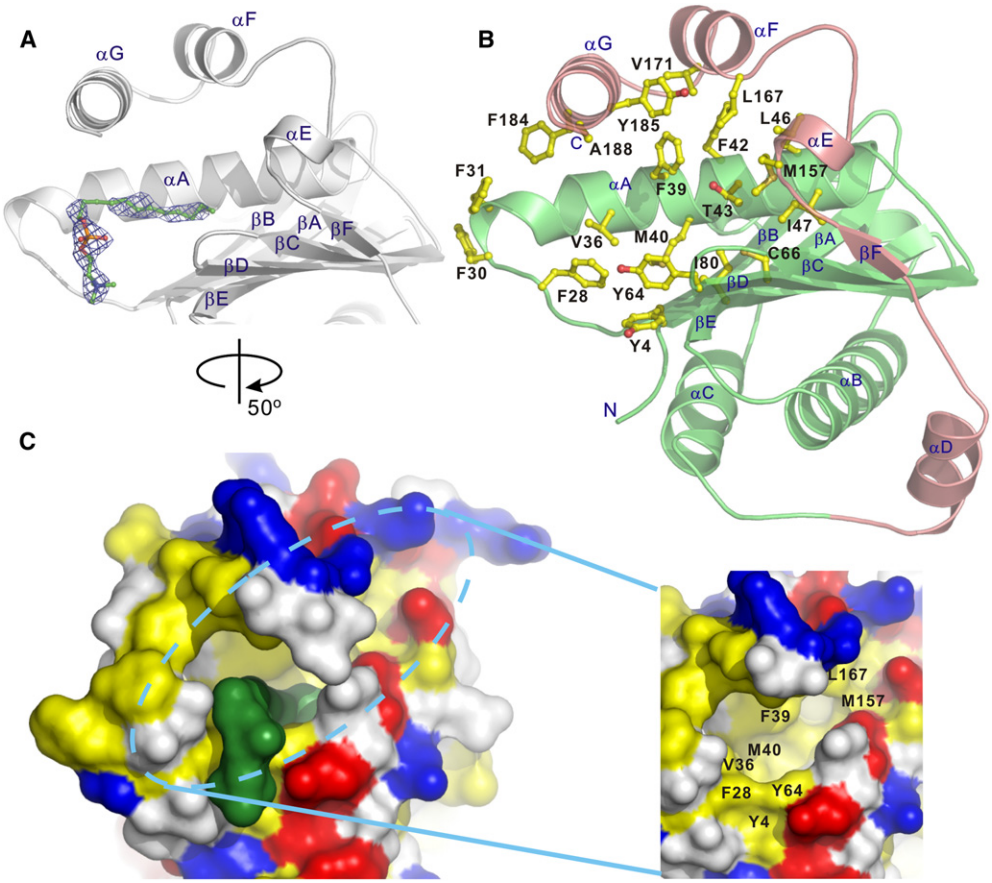

Figure 5. The DPC Binding Pocket of rYkt6

(A) Close-up view of rYkt6ΔC/DPC complex. The $2F_o - F_c$ map for the DPC molecule is drawn in blue. The omit map is calculated at 2.4 Å resolution data set and contoured at 0.8 σ. The aliphatic tails of the DPC molecule are drawn in green. The oxygen atoms of DPC are drawn in red, nitrogen atoms in blue, and phosphorus atoms in gold.

(B) The explicit atomic representation of the DPC-binding hydrophobic groove of rYkt6ΔC.

(C) Surface diagram of rYkt6ΔC/DPC complex with 50° rotation as in (A) (see also Figure S3). The positively charged amino acids are highlighted in blue, the negatively charged residues in red, the hydrophobic residues in yellow, and the others in white. The DPC molecule is shown using the space-filled model in green and purple, respectively. The semiopen hydrophobic groove that accommodates the DPC molecules is highlighted with a dashed oval, and the groove with DPC removed is shown as an enlarged insert. For clearance, the last residue, Asn192, is removed from the figure.

(Figure 7G). Fully consistent with the membrane localization data, all of the four Ykt6 mutants (F42E, V171E, Y64E, and Y185E) showed much higher capacities in binding to Bet1 than the wild-type Ykt6, again due to the mutation-induced opening of the SNARE core of the Ykt6 mutants. As the control, neither the wild-type Ykt6 nor its mutants pulled down Sec22b, another longin SNARE that is known not to form complex with Ykt6 or Bet1 (Zhang and Hong, 2001). We have also probed the possible interaction of the Ykt6 mutants with a plasma membrane SNARE syntaxin 4, since the Ykt6 mutants are found in membrane compartments other than Golgi apparatus (Figures 7B–7E). Neither the wild-type nor the mutant forms of Ykt6 interacted with syntaxin 4 (Figure 7G), indicating that the conformation opening of Ykt6 leads to enhanced reactivity for

(C) Surface presentation showing the longin domain/SNARE core interaction of Ykt6. For clarity, two panels are used, with each panel showing one domain in the surface representation and the other in the ribbon diagram.

(D) Superposition of the longin domains of rYkt6 (green), Sec22b (orange), and VAMP7 (blue, in complex with Hrb) with the SNARE motifs of rYkt6 and Sec22b in pink and orange, respectively. The Hrb fragment in the VAMP7/Hrb complex is drawn in blue. The "APTLHL" motif of Hrb is shown in explicit atom presentation. The common structural elements in the core regions (i.e., a β strand followed by a short α helix, βF–αE in rYkt6) shared by all three longin SNAREs are highlighted with a red dashed circle.

(E) Structural-based amino acid sequence alignment of rYkt6, Sec22b, and VAMP7 showing that the residues involved in the interactions highlighted with the red circle in (D) are highly conserved among all three longin SNARES (see also Figure S2). For comparison, the corresponding sequence of the Hrb fragment in the VAMP7/Hrb complex is also included. In this alignment, the amino acid residues involved in the interdomain interactions are shown in blue.

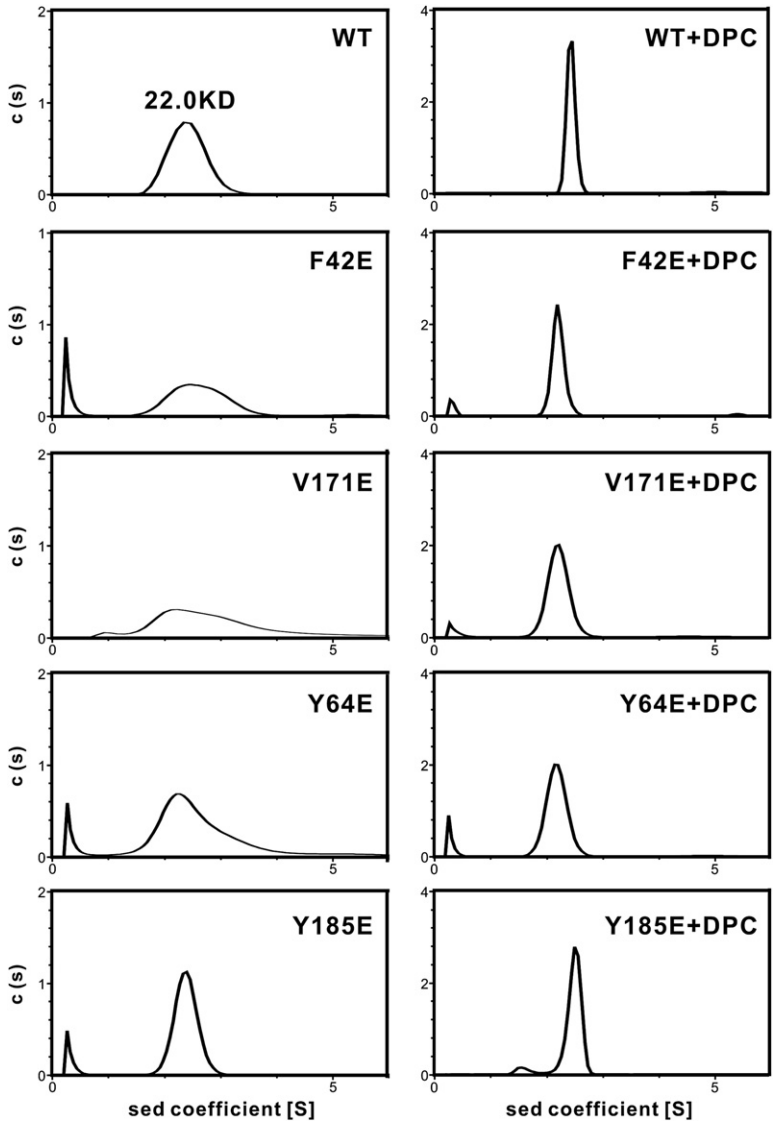

Figure 6. Analytical Ultracentrifugation Profiles of the Wild-Type rYkt6ΔC and Its Various Mutants (~40 μM) in the Absence and Presence of 0.6 mM DPC

The sedimentation velocity data of different forms of rYkt6ΔC were fitted to a continuous sedimentation coefficient distribution model with the fitted curves shown as solid lines. The calculated molecular weight for the wild-type rYkt6ΔC is indicated at top of the figure. The buffer condition was identical to that used in NMR experiments. See also Figure S4 for related experiments.

its cognate SNAREs but does not change its SNARE binding specificity.

DISCUSSION

Among the various SNAREs that play critical roles in determining specific membrane fusion events, Ykt6 is exceptional due to its unique subcellular distributions. Despite its localization in both the cytoplasm and membranes, the function of Ykt6 seems to be restricted to membranes, and the majority of Ykt6 in its resting state resides in the cytosol. The dynamics of Ykt6 are believed to be governed by the reversible palmitoylation of the protein, which cycles Ykt6 between intracellular membranes and the cytoplasm (Fukasawa et al., 2004; McNew et al., 1997; Meiringer et al., 2008), although it was not clear why farnesylation alone cannot bring Ykt6 to membranes. The results presented here provide a clear answer to the above question. In farnesylated, unpalmitoylated Ykt6, the longin domain, the SNARE core, and the farnesyl group function cooperatively to keep the protein in its water-soluble conformation by sequestering the lipid group inside the hydrophobic pocket formed by the extensive interactions between the longin domain and the SNARE core. In return, the farnesyl group plays a vital role in stabilizing the closed conformation of Ykt6 and ensures that the SNARE core of Ykt6 does not open to pair with other SNAREs (Figure 7H). This tightly regulated closed conformation of Ykt6 is likely to be important, as otherwise Ykt6 may pair with many other SNAREs nonspecifically due to its ubiquitous cytoplasmic localization. Palmitoylation of Ykt6 increases the partition coefficient of the double-lipidated protein to membranes, thereby shifting some populations of the protein from the cytosol to cellular membranes (Fukasawa et al., 2004; Hasegawa et al., 2004; Meiringer et al., 2008) (Figure 7H). It is likely that palmitoylation-mediated membrane insertion will further shift the conformational equilibrium of Ykt6 to the open state due to the increased membrane insertion propensity of the farnesyl group (Figure 7H). The specific membrane localization and the amount of membrane-associated Ykt6 are predicted to be affected by its reversible palmitoylation machinery in cells, as the majority of Ykt6 exists in the unpalmitoylated cytosolic form (Meiringer et al., 2008).

The farnesyl-mediated conformational and fusion activity regulation of Ykt6 indicates that posttranslationally attached lipid can directly regulate the activities of the lipid-modified proteins in addition to their well-known membrane-anchoring roles. It has been well documented that lipid moieties alone or together with other regulatory processes (e.g., via binding to ligands/proteins, phosphorylation, etc.) can dynamically regulate membrane binding as well as targeting to various membrane environments of acylated and/or prenylated proteins (Linder and Deschenes, 2007; Pylypenko et al., 2008; Resh, 2006). Direct regulations of biological activities of protein by posttranslationally attached lipid moieties are much less documented. It will be interesting to explore in the future whether direct activity regulation of proteins

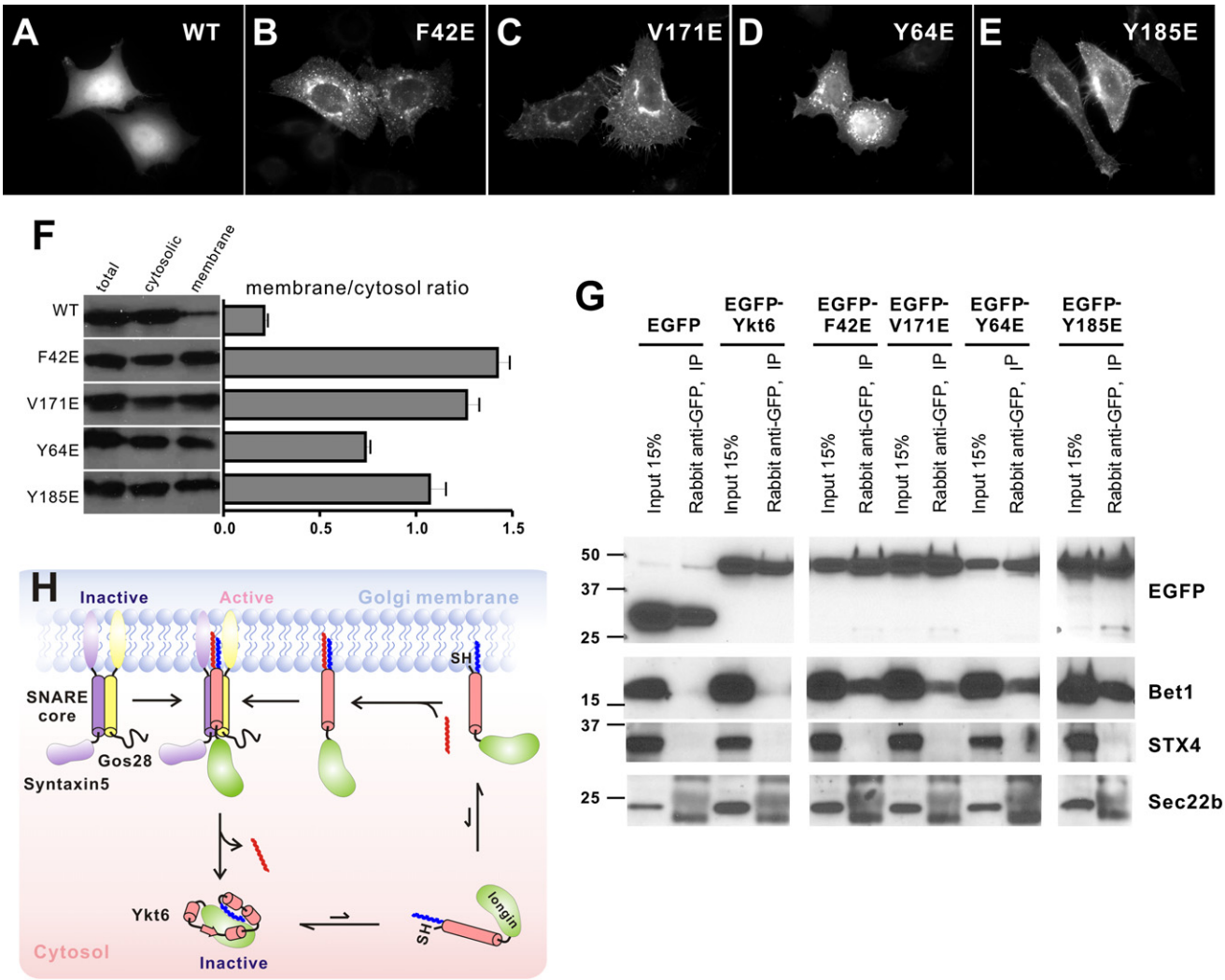

Figure 7. Intracellular Localization and SNARE Complex Assembly of GFP-Tagged rYkt6 and Its Mutants Transiently Expressed in HeLa Cells

(A–E) Cells were transiently transfected with GFP-tagged wild-type rYkt6 (A), rYkt6-F42E (B), rYkt6-V171E (C), rYkt6-Y64E (D), and rYkt6-Y185E (E).

(F) Subcellular fractionation of the wild-type Ykt6 and its mutants showing that the Ykt6 mutants shown in (B)–(E) are mainly bound to membranes. The membrane/cytosolic ratios of the wild-type Ykt6 and each of its mutants were quantified. Values are mean ±SD of three different experiments.

(G) The Ykt6 mutants with open conformations have higher capacity in binding to cognate SNARE Bet1 than the wild-type protein. Sec22b, another longin SNARE protein, was used as the negative control. The figure also shows that neither the wild-type nor its conformation opening mutants bind to the plasma membrane SNARE syntaxin 4 (STX4).

(H) A schematic model depicting the lipidation-dependent cytoplasm membrane shuttling of Ykt6 in cells.

by attached lipids (e.g., inhibition of the SNARE core fusion activity of Ykt6) is a rather common property of a subset among the huge collection of proteins that can be posttranslationally modified by lipids (Kang et al., 2008; Nguyen et al., 2009; Roth et al., 2006).

In summary, we have demonstrated that the single lipidation (i.e., farnesylation) of Ykt6 shifts the conformation of the longin SNARE from a semiclosed state into a dominantly closed and fusion-inactive state through the coordinated actions of the longin domain, the SNARE core, and the lipid molecule. This autoinhibited, closed conformation of Ykt6 can be relieved by further lipidation (i.e., palmitoylation) of the protein. The results described here demonstrate that lipid molecules can actively and dynamically regulate protein activities in addition to their well-known passive membrane-anchoring roles.

EXPERIMENTAL PROCEDURES

Protein Expression and Purification

DNA sequences encoding rYkt6 longin domain (residues 1–137, rYkt6N), rYkt6ΔC (residues 1–193), and the full-length rYkt6 (residues 1–198) were individually cloned into a modified version of pET32a vector. All point mutations of rYkt6 used in this study were created using the standard PCR-based mutagenesis method and confirmed by DNA sequencing. Recombinant proteins were expressed in *Escherichia coli* BL21 (DE3) host cells at 16°C. His_6-tagged rYkt6 proteins expressed in bacterial cells were purified by Ni^{2+}-NTA agarose affinity

chromatography followed by size-exclusion chromatography. Uniformly ^{15}N- or ^{15}N,^{13}C-labeled rYkt6 proteins were prepared by growing bacteria in M9 minimal medium using $^{15}NH_4Cl$ as the sole nitrogen source or $^{15}NH_4Cl$ and $^{13}C_6$-glucose as the sole nitrogen and carbon sources, respectively.

NMR Experiments

All protein samples for NMR titration experiments were concentrated to ~0.2 mM in 50 mM Tris (pH 7.0, with 1 mM DTT, 1 mM EDTA, and 100 mM NaCl). NMR spectra were acquired at 30°C on Varian Inova 500 MHz or 750 MHz spectrometers. Backbone resonance assignments of rYkt6N were achieved by standard heteronuclear correlation experiments, including HNCO, HNCACB, and CBCA(CO)NH using a ~1 mM ^{15}N/^{13}C-labeled protein sample (Bax and Grzesiek, 1993).

Crystallography

Crystals of rYkt6ΔC were obtained by the hanging-drop vapor diffusion method at 16°C. Freshly purified rYkt6ΔC was concentrated to 0.35 mM before a saturating amount of DPC lipid (up to three molar ratio of the lipid to rYkt6ΔC) was added. The rYkt6ΔC/DPC mixture was set up in hanging drops with equal volumes of 2 M $(NH_4)_2SO_4$ and 0.1 M Tris (pH 8.5). Glycerol (20%, v/v) was used as the cryoprotectant for the Ykt6 crystals. The final refinement statistics are listed in Table 1.

Analytical Ultracentrifugation

Sedimentation velocity experiments were performed on a Beckman XL-I analytical ultracentrifuge equipped with an eight-cell rotor at 25°C. The partial specific volume of protein samples and the buffer density were calculated using the program SEDNTERP (http://www.rasmb.bbri.org/). The final sedimentation velocity data were analyzed using the program SEDFIT (http://www.analyticalultracentrifugation.com/).

Cell Culture, Immunostaining, and Imaging

HeLa cells were cultured in MEM media supplemented with fetal bovine serum. For immunostaining, cells were cultured on coverslips coated with 0.2% gelatin. The cDNA encoding the N-terminal GFP-tagged wild-type or mutant rYkt6 cloned into the pEGFP vector were individually introduced into cells by the Lipofectamine transfection method. The cells were fixed at 36–48 hr after transfection by 4% paraformaldehyde and 4% sucrose in PBS, then permeabilized by 0.2% Triton X-100 in PBS for 10 min at room temperature. The cells were imaged with a Nikon Eclipse TE2000 (Nikon, Tokyo) inverted fluorescence microscope.

Subcellular Fractionations of the Wild-Type Ykt6 and Its Mutations

Cells expressed with the GFP-tagged wild-type rYkt6 or its mutants were harvested and then homogenized in HEPES buffer (20 mM HEPES, 100 mM NaCl, 5 mM $MgCl_2$, 1 mM DTT, 5 mM sucrose, 1 mM PMSF [pH 7.5]) 30 hr after transfection. A postnuclear supernatant was obtained by spinning each cell lysate at 600 × *g* for 10 min. The resulting supernatant was then subjected to centrifugation at 100,000 × *g* for 1 hr to separate cytosol and membrane fractions. Equal amount of protein loading was shown by the total GFP-tagged rYkt6 or its mutants detected by western blot using the anti-GFP antibody.

SNARE Assembly Assay

Cells expressed with the GFP-tagged wild-type rYkt6 or its mutants were lysed in 50 mM Tris-HCl buffer (pH 7.5) containing 150 mM NaCl, 1% Triton X-100, and protease inhibitors. The Ykt6-assembled SNARE complexes were precipitated with anti-GFP antibody. Ykt6 in the precipitated SNARE complex was immunodetected using the anti-GFP antibody; Bet1 and syntaxin 4 were visualized by western blot using anit-Bet1 and anti-syntaxin 4 antibodies, respectively (Zhang and Hong, 2001).

ACCESSION NUMBERS

The atomic coordinates of rYkt6ΔC/DPC complex have been deposited in the Protein Data Bank under the accession code 3KYQ.

SUPPLEMENTAL INFORMATION

Supplemental Information includes Supplemental Experimental Procedures, Supplemental References, and four figures and can be found with this article online at doi:10.1016/j.molcel.2010.01.024.

ACKNOWLEDGMENTS

We thank Hao Wu, Cong Yu, and Ling-Nga Chan for technical assists; Yanxiang Zhao for collecting the X-ray diffraction data; and Anthony Zhang for the critical reading of the manuscript. This work was supported by grants from the Research Grants Council of Hong Kong to M.Z. (HKUST6442/06M, 663407, 663808, CA07/08.SC01, AoE/B-15/01-II, and AoE/M-04/04), the National High Technology Research Program (2006AA02A320), the National Major Basic Research Program (2009CB918600), and NSF (Grant No. 30970574) of China.

Received: January 30, 2009
Revised: May 1, 2009
Accepted: December 29, 2009
Published: February 11, 2010

REFERENCES

Bax, A., and Grzesiek, S. (1993). Methodological advances in protein NMR. Acc. Chem. Res. *26*, 131–138.

Das, A.K., and Hajra, A.K. (1992). Critical micellar concentrations of palmitoyl dehydroxyacetone phosphate and 1-palmitoyl-rac-glycerol 3-phosphate. J. Biol. Chem. *267*, 9731.

Dietrich, L.E., and Ungermann, C. (2004). On the mechanism of protein palmitoylation. EMBO Rep. *5*, 1053–1057.

Dietrich, L.E., Gurezka, R., Veit, M., and Ungermann, C. (2004). The SNARE Ykt6 mediates protein palmitoylation during an early stage of homotypic vacuole fusion. EMBO J. *23*, 45–53.

Dilcher, M., Köhler, B., and von Mollard, G.F. (2001). Genetic interactions with the yeast Q-SNARE VTI1 reveal novel functions for the R-SNARE YKT6. J. Biol. Chem. *276*, 34537–34544.

Dominguez, C., Boelens, R., and Bonvin, A.M. (2003). HADDOCK: a protein-protein docking approach based on biochemical or biophysical information. J. Am. Chem. Soc. *125*, 1731–1737.

Dulubova, I., Sugita, S., Hill, S., Hosaka, M., Fernandez, I., Südhof, T.C., and Rizo, J. (1999). A conformational switch in syntaxin during exocytosis: role of munc18. EMBO J. *18*, 4372–4382.

Fiebig, K.M., Rice, L.M., Pollock, E., and Brunger, A.T. (1999). Folding intermediates of SNARE complex assembly. Nat. Struct. Biol. *6*, 117–123.

Fukasawa, M., Varlamov, O., Eng, W.S., Söllner, T.H., and Rothman, J.E. (2004). Localization and activity of the SNARE Ykt6 determined by its regulatory domain and palmitoylation. Proc. Natl. Acad. Sci. USA *101*, 4815–4820.

Gonzalez, L.C., Jr., Weis, W.I., and Scheller, R.H. (2001). A novel snare N-terminal domain revealed by the crystal structure of Sec22b. J. Biol. Chem. *276*, 24203–24211.

Hasegawa, H., Zinsser, S., Rhee, Y., Vik-Mo, E.O., Davanger, S., and Hay, J.C. (2003). Mammalian ykt6 is a neuronal SNARE targeted to a specialized compartment by its profilin-like amino terminal domain. Mol. Biol. Cell *14*, 698–720.

Hasegawa, H., Yang, Z., Oltedal, L., Davanger, S., and Hay, J.C. (2004). Intramolecular protein-protein and protein-lipid interactions control the conformation and subcellular targeting of neuronal Ykt6. J. Cell Sci. *117*, 4495–4508.

Jahn, R., and Scheller, R.H. (2006). SNAREs—engines for membrane fusion. Nat. Rev. Mol. Cell Biol. *7*, 631–643.

Kang, R., Wan, J., Arstikaitis, P., Takahashi, H., Huang, K., Bailey, A.O., Thompson, J.X., Roth, A.F., Drisdel, R.C., Mastro, R., et al. (2008). Neural palmitoyl-proteomics reveals dynamic synaptic palmitoylation. Nature *456*, 904–909.

Kweon, Y., Rothe, A., Conibear, E., and Stevens, T.H. (2003). Ykt6p is a multifunctional yeast R-SNARE that is required for multiple membrane transport pathways to the vacuole. Mol. Biol. Cell *14*, 1868–1881.

Linder, M.E., and Deschenes, R.J. (2007). Palmitoylation: policing protein stability and traffic. Nat. Rev. Mol. Cell Biol. *8*, 74–84.

Liu, Y., Flanagan, J.J., and Barlowe, C. (2004). Sec22p export from the endoplasmic reticulum is independent of SNARE pairing. J. Biol. Chem. *279*, 27225–27232.

Lupashin, V.V., Pokrovskaya, I.D., McNew, J.A., and Waters, M.G. (1997). Characterization of a novel yeast SNARE protein implicated in Golgi retrograde traffic. Mol. Biol. Cell *8*, 2659–2676.

Mancias, J.D., and Goldberg, J. (2007). The transport signal on Sec22 for packaging into COPII-coated vesicles is a conformational epitope. Mol. Cell *26*, 403–414.

Martinez-Arca, S., Rudge, R., Vacca, M., Raposo, G., Camonis, J., Proux-Gillardeaux, V., Daviet, L., Formstecher, E., Hamburger, A., Filippini, F., et al. (2003). A dual mechanism controlling the localization and function of exocytic v-SNAREs. Proc. Natl. Acad. Sci. USA *100*, 9011–9016.

McNew, J.A., Sogaard, M., Lampen, N.M., Machida, S., Ye, R.R., Lacomis, L., Tempst, P., Rothman, J.E., and Söllner, T.H. (1997). Ykt6p, a prenylated SNARE essential for endoplasmic reticulum-Golgi transport. J. Biol. Chem. *272*, 17776–17783.

Meiringer, C.T., Auffarth, K., Hou, H., and Ungermann, C. (2008). Depalmitoylation of Ykt6 prevents its entry into the multivesicular body pathway. Traffic *9*, 1510–1521.

Misura, K.M., Scheller, R.H., and Weis, W.I. (2000). Three-dimensional structure of the neuronal-Sec1-syntaxin 1a complex. Nature *404*, 355–362.

Munson, M., Chen, X., Cocina, A.E., Schultz, S.M., and Hughson, F.M. (2000). Interactions within the yeast t-SNARE Sso1p that control SNARE complex assembly. Nat. Struct. Biol. *7*, 894–902.

Nguyen, U.T., Guo, Z., Delon, C., Wu, Y., Deraeve, C., Fränzel, B., Bon, R.S., Blankenfeldt, W., Goody, R.S., Waldmann, H., et al. (2009). Analysis of the eukaryotic prenylome by isoprenoid affinity tagging. Nat. Chem. Biol. *5*, 227–235.

Nicholson, K.L., Munson, M., Miller, R.B., Filip, T.J., Fairman, R., and Hughson, F.M. (1998). Regulation of SNARE complex assembly by an N-terminal domain of the t-SNARE Sso1p. Nat. Struct. Biol. *5*, 793–802.

Pryor, P.R., Jackson, L., Gray, S.R., Edeling, M.A., Thompson, A., Sanderson, C.M., Evans, P.R., Owen, D.J., and Luzio, J.P. (2008). Molecular basis for the sorting of the SNARE VAMP7 into endocytic clathrin-coated vesicles by the ArfGAP Hrb. Cell *134*, 817–827.

Pylypenko, O., Schönichen, A., Ludwig, D., Ungermann, C., Goody, R.S., Rak, A., and Geyer, M. (2008). Farnesylation of the SNARE protein Ykt6 increases its stability and helical folding. J. Mol. Biol. *377*, 1334–1345.

Resh, M.D. (2006). Trafficking and signaling by fatty-acylated and prenylated proteins. Nat. Chem. Biol. *2*, 584–590.

Rossi, V., Banfield, D.K., Vacca, M., Dietrich, L.E., Ungermann, C., D'Esposito, M., Galli, T., and Filippini, F. (2004). Longins and their longin domains: regulated SNAREs and multifunctional SNARE regulators. Trends Biochem. Sci. *29*, 682–688.

Roth, A.F., Wan, J., Bailey, A.O., Sun, B., Kuchar, J.A., Green, W.N., Phinney, B.S., Yates, J.R., 3rd, and Davis, N.G. (2006). Global analysis of protein palmitoylation in yeast. Cell *125*, 1003–1013.

Rys-Sikora, K.E., and Gill, D.L. (1998). Fatty acid-mediated calcium sequestration within intracellular calcium pools. J. Biol. Chem. *273*, 32627–32635.

Söllner, T., Whiteheart, S.W., Brunner, M., Erdjument-Bromage, H., Geromanos, S., Tempst, P., and Rothman, J.E. (1993). SNAP receptors implicated in vesicle targeting and fusion. Nature *362*, 318–324.

Südhof, T.C., and Rothman, J.E. (2009). Membrane fusion: grappling with SNARE and SM proteins. Science *323*, 474–477.

Sutton, R.B., Fasshauer, D., Jahn, R., and Brunger, A.T. (1998). Crystal structure of a SNARE complex involved in synaptic exocytosis at 2.4 A resolution. Nature *395*, 347–353.

Tochio, H., Tsui, M.M., Banfield, D.K., and Zhang, M. (2001). An autoinhibitory mechanism for nonsyntaxin SNARE proteins revealed by the structure of Ykt6p. Science *293*, 698–702.

Ungermann, C., von Mollard, G.F., Jensen, O.N., Margolis, N., Stevens, T.H., and Wickner, W. (1999). Three v-SNAREs and two t-SNAREs, present in a pentameric cis-SNARE complex on isolated vacuoles, are essential for homotypic fusion. J. Cell Biol. *145*, 1435–1442.

Weber, T., Zemelman, B.V., McNew, J.A., Westermann, B., Gmachl, M., Parlati, F., Söllner, T.H., and Rothman, J.E. (1998). SNAREpins: minimal machinery for membrane fusion. Cell *92*, 759–772.

Wen, W., Chen, L., Wu, H., Sun, X., Zhang, M., and Banfield, D.K. (2006). Identification of the yeast R-SNARE Nyv1p as a novel longin domain-containing protein. Mol. Biol. Cell *17*, 4282–4299.

Zhang, T., and Hong, W. (2001). Ykt6 forms a SNARE complex with syntaxin 5, GS28, and Bet1 and participates in a late stage in endoplasmic reticulum-Golgi transport. J. Biol. Chem. *276*, 27480–27487.